

Quadratic Pulse Inversion Ultrasonic Imaging (QPI): Analysis and Design of Quadratic Kernel in the Frequency Domain to reduce tissue component introduced by motion

Mamoun F. Al-Mistarihi, Electrical Engineering Department, Jordan University of Science and Technology, Irbid, Jordan *and* *Emad S. Ebbini*, Department of Electrical and Computer Engineering, University of Minnesota, Minneapolis, MN 55455

ABSTRACT

We have previously introduced an ultrasonic imaging approach that combines harmonic-sensitive pulse sequences with a post-beamforming quadratic kernel derived from SOVF. The approach was designed to produce images with high sensitivity to nonlinear oscillations (20 – 30 dB below the fundamental) from microbubble ultrasound contrast agents (UCA) while maintaining high levels of noise rejection. Although pulse inversion detection using the sum signal, can detect the nonlinear echoes from micrbubbles and suppress the linear echoes from stationary tissue, echoes from moving tissue will not be suppressed completely and could mask echoes from microbubbles. In this paper, analysis and design of the quadratic kernel in the frequency domain for the case of linear scatterer motion is presented leading to reduction of tissue component introduced by motion and increase the specificity while optimizing the sensitivity to the ultrasound contrast agents (UCA). The approach is demonstrated experimentally using images from imaging flow phantom under a variety of exposure conditions and UCA concentration levels. Imaging results show a significant increase in harmonic sensitivity, reduction in noise levels and reduction of tissue component introduced by motion.

1. INTRODUCTION

Microbubble ultrasound contrast agents (UCA) are being investigated for use in clinical imaging applications for tissue function and for targeted therapeutic applications. The objective is to detect minute concentrations of UCA in the microvasculature during ultrasonic exams thus providing a view of the perfusion in the tissue. This functional form of ultrasonic imaging is seen an important component for the continued use of ultrasound as a medical imaging modality. For example, many tumors without distinguishing characteristics on conventional ultrasound have characteristic blood perfusion patterns that allow for easy detection if a perfusion sensitive imaging is available.

Interaction between microbubbles UCAs and acoustic wave result in nonlinear harmonic echo generation. This phenomenon can be exploited to enhance the echoes from the microbubbles and, therefore, reject fundamental components resulting largely from tissue. Imaging techniques based on nonlinear oscillations have been designed for separating and enhancing nonlinear UCA echoes from a specified region of interest within the imaging field, including second harmonic (SH) imaging and pulse inversion (PI) Doppler imaging [1]. The SH imaging employs a fundamental frequency transmit pulse and produces images from the second harmonic component of received echoes by using a second harmonic bandpass filter (BPF) to remove the fundamental frequency. In order to increase UCA detection

sensitivity in the limited transducer bandwidth condition, spectral overlap between fundamental and second harmonic parts need to be minimized by transmitting narrow-band pulses resulting in an inherent tradeoff between contrast and spatial resolution. In PI imaging a sequence of two inverted acoustic pulses with appropriate delay is transmitted into tissue. Images are produced by summing the corresponding two backscattered signals. In the absence of tissue motion, the resulting sum can be shown to contain only even harmonics of the nonlinear echoes. The PI imaging overcomes the tradeoff between contrast and spatial resolution because it utilizes the entire bandwidth of the backscattered signals. As a result, superior spatial resolution can be achieved when compared with SH imaging. However, the subtraction process results in significant reduction of signal to noise as the harmonics are typically 20 - 30 dB or more below the (cancelled) fundamental component.

We have previously shown that the SOVF-based quadratic kernels provide high sensitivity to harmonic echoes comparable to PI with a significant increase in dynamic range due to inherent noise rejection of quadratic filtering [2]. An algorithm for deriving the coefficients of the kernel using singular values decomposition (SVD) of a linear and quadratic prediction data matrix was proposed and experimentally validated in [3]. Imaging results and comparisons with SH and PI images have shown that quadratic imaging is superior to SH and compares favorably with PI without the need for multiple transmissions. However, due to reliance on linear and quadratic prediction, the quadratic kernel has sensitivity to the fundamental that limits its ability to detect UCA in the microvasculature.

Although pulse inversion detection using the sum signal, can detect the nonlinear echoes from micrbubbles and suppress the linear echoes from stationary tissue, echoes from moving tissue will not be suppressed completely and could mask echoes from microbubbles. This paper combines PI and quadratic imaging to mitigate the limitations of both methods. The approach is based on quadratic filtering of PI data that, while noisy, is largely free of fundamental stationary tissue components. The efficiency of the quadratic kernel in rejecting noise while maintaining quadratic signal components allows the recovery of quadratic components below the noise floor. This new quadratic PI (QPI) imaging approach offers the promise of detecting harmonic oscillations at or below the noise floor. Given the current trend of imaging UCA with extremely low transmit pulse amplitudes (to minimize nonlinear echo generation from tissue), the ability of QPI to detect quadratic signal activity below the noise floor becomes essential to the detection of harmonic activity in the 40 – 50 dB range below the fundamental.

Analysis and design of the quadratic kernel in the frequency domain for the case of linear scatterer motion is presented. The imaging results given in this paper indicate that a signal processing approach to this clinical challenge is feasible.

2. THEORY

The algorithm in this section is based on [2-4], which have shown the validity of a SOVF as a model for pulse-echo ultrasound data from tissue mimicking media. The response of a quadratically nonlinear system with memory $\hat{y}(n+1)$, can be predicted by a second order Volterra model of m past values as follows:

$$\hat{y}(n+1) = \sum_{j=0}^{m-1} y(n-j)h_L(i) + \sum_{j=0}^{m-1} \sum_{k=j}^{m-1} y(n-j)y(n-k)h_Q(j,k) \quad (1)$$

where $h_L(i)$ and $h_Q(j,k)$ are the linear and quadratic filter coefficients, respectively. Using a segment of the RF data, a system of linear equations are formed and solved for elements of the quadratic kernel. Details of the algorithm to determine the quadratic kernel that provide maximum contrast enhancement have been described in [2-4].

In this paper, we present a new algorithm of post beamforming second order Volterra filter on a pulse inversion data (QPI) leading to reduction of tissue component introduced by motion and increase the specificity while optimizing the sensitivity to the ultrasound contrast agents (UCA). Applying quadratic filtering to Pulse-inversion data (in that order) allows the cascade to efficiently mitigate the limitations of either imaging method applied alone.

Using the second-order frequency response (SFR), i.e. $H(e^{jw_1}, e^{jw_2})$, of the quadratic kernel, we are able to design a new quadratic kernel that offers higher sensitivity to UCA signals while minimizing the effect of the linear signal introduced by motion using a gain function which has minimum values at the frequencies with high values of linear-to-tissue ratio (LTR).

Based on ratio of contrast-to-tissue magnitude and linear-to-tissue magnitude in the (w_1, w_2) domain which are

$$CTR(e^{jw_1}, e^{jw_2}) = \frac{\overline{|H|}_{CT}(e^{jw_1})\overline{|H|}_{CT}(e^{jw_2})}{\overline{|H|}_{TS}(e^{jw_1})\overline{|H|}_{TS}(e^{jw_2})} \quad (2)$$

$$LTR(e^{jw_1}, e^{jw_2}) = \frac{\overline{|H|}_{LS}(e^{jw_1})\overline{|H|}_{LS}(e^{jw_2})}{\overline{|H|}_{TS}(e^{jw_1})\overline{|H|}_{TS}(e^{jw_2})} \quad (3)$$

where $\overline{|H|}_{CT}(\bullet)$, $\overline{|H|}_{LS}(\bullet)$ and $\overline{|H|}_{TS}(\bullet)$ are the average magnitude of frequency responses of RF data in UCA, linear scatterer and tissue regions, respectively we introduce the following gain functions:

- The $G_{CTR}(e^{jw_1}, e^{jw_2})$ gain is designed for improving sensitivity to UCA. This can be achieved by amplifying gains of the quadratic kernel in the (w_1, w_2) plane where components from UCA are higher than those from tissue. $G_{CTR}(e^{jw_1}, e^{jw_2})$ is expressed by

$$G_{CTR}(e^{jw_1}, e^{jw_2}) = \begin{cases} 1 & : CTR < \lambda_1 \\ \frac{\overline{|H|}_{CT}(e^{jw_1})\overline{|H|}_{CT}(e^{jw_2})}{\overline{|H|}_{TS}(e^{jw_1})\overline{|H|}_{TS}(e^{jw_2})} & : CTR > \lambda_1 \end{cases} \quad (4)$$

- The $G_{LTR}(e^{jw_1}, e^{jw_2})$ gain is designed for minimizing sensitivity to the linear scatterer. This can be achieved by minimizing gains of the quadratic kernel in the (w_1, w_2) plane where components from the linear scatterer are higher than those from tissue. $G_{LTR}(e^{jw_1}, e^{jw_2})$ is expressed by

$$G_{LTR}(e^{jw_1}, e^{jw_2}) = \begin{cases} 1 & : LTR < \lambda_2 \\ \frac{1}{\sqrt{\frac{\overline{|H|}_{LS}(e^{jw_1})\overline{|H|}_{LS}(e^{jw_2})}{\overline{|H|}_{TS}(e^{jw_1})\overline{|H|}_{CT}(e^{jw_2})}}} & : LTR > \lambda_2 \end{cases} \quad (5)$$

The overall gain function used to modify the quadratic kernel is expressed by

$$G(e^{jw_1}, e^{jw_2}) = \begin{cases} 1 & : CTR < \lambda_1 \\ G_{CTR}(e^{jw_1}, e^{jw_2}) & : CTR > \lambda_1 \cap LTR < \lambda_2 \\ \frac{G_{LTR}(e^{jw_1}, e^{jw_2})}{G_{CTR}(e^{jw_1}, e^{jw_2})} & : CTR > \lambda_1 \cap LTR > \lambda_2 \end{cases} \quad (6)$$

The modified quadratic kernel is determined from the inverse DTFT of

$$H_{modified}(e^{jw_1}, e^{jw_2}) = \begin{cases} H(e^{jw_1}, e^{jw_2}) & : CTR > \lambda_1 \\ G_{CTR}(e^{jw_1}, e^{jw_2})H(e^{jw_1}, e^{jw_2}) & : CTR > \lambda_1 \cap LTR < \lambda_2 \\ \frac{G_{LTR}(e^{jw_1}, e^{jw_2})}{G_{CTR}(e^{jw_1}, e^{jw_2})}H(e^{jw_1}, e^{jw_2}) & : CTR > \lambda_1 \cap LTR > \lambda_2 \end{cases} \quad (7)$$

where $H(e^{jw_1}, e^{jw_2})$ is the SFR of the quadratic kernel, λ_1 and λ_2 are contrast-to-tissue and linear-to-tissue values, respectively, chosen as a threshold values in the quadratic kernel design.

3. EXPERIMENTAL SETUP

To demonstrate generality and robustness of the new approach, a flow phantom, shown in Figure 1, (Model 524; ATS Laboratories, Inc., Bridgeport, CT) containing four flow channels with diameters 2, 4, 6, and 8 mm embedded in rubber-based tissue mimicking material was used in obtaining the images. The flow phantom was connected to a flow system with a roller pump (Model 77200-60; Cole-Parmer Instrument Co., Vernon Hills, IL). Subsequently, the diluted BR14 was circulated. In addition, the diluted BR14 and the linear scatterer were constantly stirred in two beakers using a magnetic hot plate stirrer (EW-84303-20; Corning Inc., Corning NY). This experiment was designed to compare PI, and QPI images of the nonlinear backscattered signals from BR14 in the 6 mm

diameter flow channel and the linear backscattered signals from cellulose type 20 in the 4 mm diameter flow channel. RF data were recorded and saved for later processing by the Technos MP ultrasound system (ESAOTE S.p.A, Genova, Italy) with a linear array probe (LA 522 E; ESAOTE S.p.A, Genova, Italy) located perpendicularly to the ultrasound contrast agent flow channel. A pair of inverted pulses at 1.56 MHz were transmitted to produce a PI image.

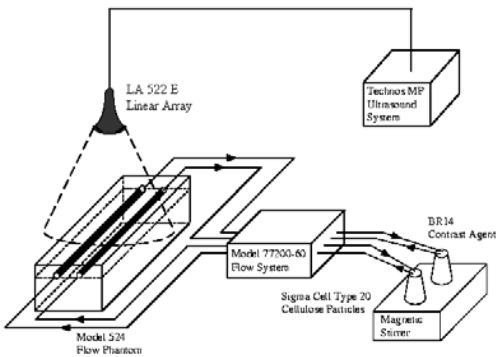


Figure 1: The imaging setup for the flow phantom

4. RESULTS AND DISCUSSION

Figure 2 shows the average spectra of typical echoes from the contrast, linear scatterer and tissue regions of the flow phantom described in Section III-A. The average spectra are calculated by averaging windowed periodogram of every echo line in regions described in Section III-D. The echoes from the UCA exhibit broader bandwidth than those from the linear scatterer and tissue regions.

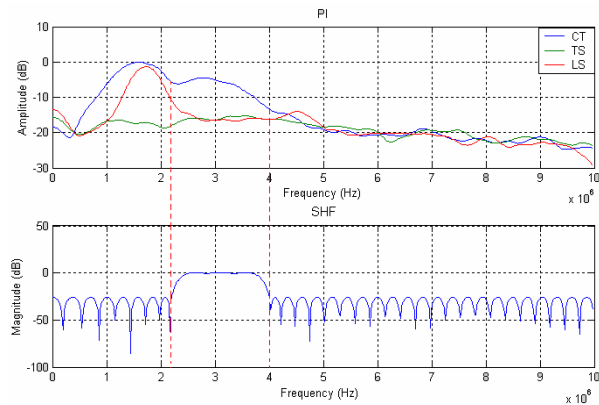


Figure 2: Average spectra from the contrast (blue), linear scatterer (red) and tissue (green) regions of the flow phantom, magnitude of frequency response of the bandpass filter.

From the figure, the UCA spectra shows spectral peaks at the fundamental and 2nd harmonic. There is a spectral peak at the fundamental from the linear scatterer because some scatterers velocities does not obey the Nyquist limit. Also, the figure shows the magnitude of frequency response of the band pass filter used to get the second-harmonic pulse inversion (SHPI) image with a center frequency 3.1 MHz and a bandwidth of 1.7 MHz.

Figure 3 shows a filled contour plot of magnitude of frequency responses in the (w_1, w_2) plane obtained using RF data in the tissue region, it was calculated using an outer product of the average tissue spectrum in 1D. The filled contour plot displays isolines calculated from the magnitude of frequency function in the (w_1, w_2) plane and fills the areas between the isolines using constant colors. We can see that the dominant peak is approximately at $(w_1, w_2) = (3.2, 3.2)$ MHz, which corresponds to the 1D spectrum shown in Figure 3. The magnitude of frequency responses obtained using RF data in the contrast region is shown. The dominant peak is approximately at $(w_1, w_2) = (1.6, 1.6)$ MHz which corresponds to the 1D spectrum too. The magnitude of frequency responses obtained using RF data in the linear scatterer region is shown. The dominant peak is approximately at $(w_1, w_2) = (1.7, 1.7)$ MHz which corresponds to the 1D spectrum too. Also, the figure shows the ratio of contrast to tissue magnitude and the ratio of linear to tissue magnitude in the (w_1, w_2) domain. Distinct peaks in the 2D plane of contrast to tissue magnitude and linear to tissue magnitude are seen at frequencies (1.6,1.6) MHz. This frequency results from interaction between magnitudes of frequency responses in 1D at 1.6 MHz where contrast magnitude is significantly higher than that from tissue. The maximum gain in the SFR of the 5th singular mode quadratic kernel is centered around (1,6,1,6) MHz.

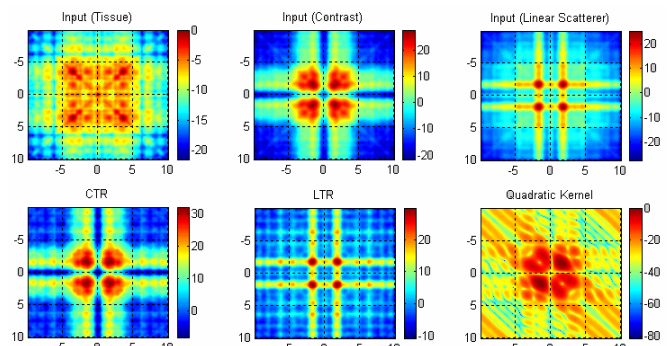


Figure 3: Filled contour plots of magnitude frequency responses in the (w_1, w_2) plane resulting from: input RF data in the tissue region, input RF data in the linear scatterer region, input RF data in the contrast region, ratio of contrast to tissue magnitude, ratio of linear to tissue magnitude, SFR of the 5th singular mode quadratic kernel

Figure 4 shows the SFR of both the quadratic kernel and the modified quadratic kernel, from the figure we can clearly see that regions where the LTR magnitude in the (w_1, w_2) plane has high values are minimized and that regions where the CTR magnitude in the (w_1, w_2) plane has high values are amplified excluding the overlap frequency region where both the CTR magnitude and LTR magnitude have high values

Figure 5 shows images of a flow phantom obtained using pulse inversion (PI), second harmonic pulse inversion (SHPI), and quadratic pulse inversion (QPI) respectively. The PI image shows the UCA in the 6-mm flow channel (left) and the linear scatterer in the 4-mm flow channel (right) surrounded by tissue-mimicking material was acquired using the experimental setup described in Section 3.

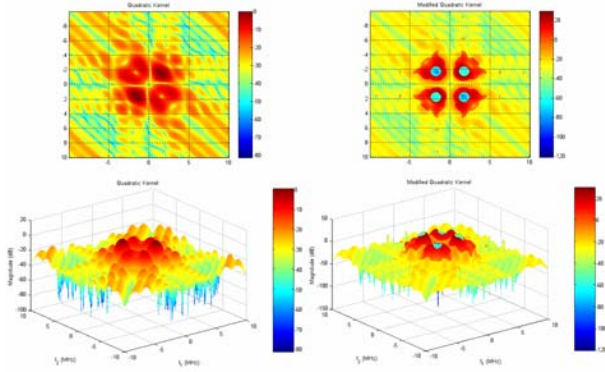


Figure 4: SFR of the Quadratic kernel and modified quadratic kernel

Due to differences in dynamic ranges, each image is displayed with its full dynamic range as can be seen from the dB-level scale bars. Although pulse inversion detection using the sum signal can detect the nonlinear echoes from microbubbles and suppress the linear echoes from stationary tissue, echoes from the linear scatterer is not suppressed completely because some of the linear scatterers velocities does not obey the Nyquist limit. Thus the signals from linear scatterers will appear shifted in the frequency spectrum which cause a portion of the linear scatterer signal appear in the sum frequency component. One can see the backscattered enhancement due to the UCA in the 6-mm flow channel compared with the surrounding tissue with CTR 20.0384 dB. There is a backscattered signal due to the linear scatterers in the 4-mm channel because some scatterer velocities does not obey the Nyquist limit, LTR 8.7695 dB.

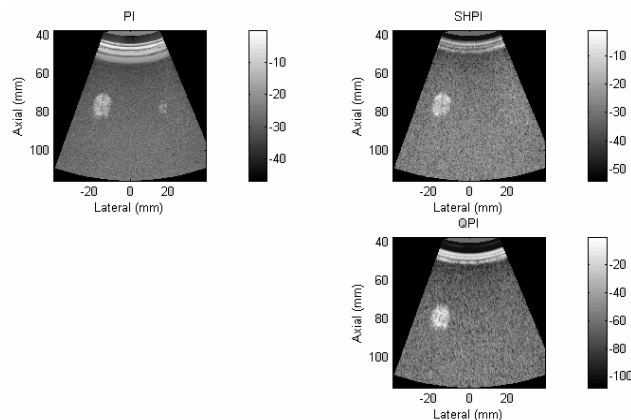


Figure 5: Images of the flow phantom using: Pulse Inversion (PI), Second Harmonic Pulse Inversion (SHPI) and Quadratic Pulse Inversion (QPI).

The second harmonic image results from filtering the PI data using a band pass filter with a center frequency at 3.1 MHz and a band width of 1.7 MHz removes the linear backscattered signal introduced by motion with LTR -0.1645 dB and CTR 10.6002 dB. One can see that there is a reduction in the CTR value compared with that of the PI image due to the removal of part of the contrast signal.

The quadratic pulse inversion, QPI, image was obtained using the algorithm described by the flowchart of Figure 1, provides CTR 28.0539 dB and LTR 0.0361 dB. These values indicates contrast enhancement over the PI and SHPI images. One important feature of the QPI image is the increased dynamic range compared to PI and SHPI images. With the use of the modified quadratic kernel whose SFR is shown in Figure 7 we were able to remove the linear backscattered signal introduced by motion.

CTR and LTR values for the flow phantom using different imaging methods are summarized in Table 1.

Table 1

CTR and CR for the different imaging methods

Imaging Method	CTR	LTR
PI	20.0384	8.7695
SHPI	10.6002	-0.1645
QPI	28.0539	0.0361

5. CONCLUSIONS

The results shown in this paper indicate clearly that QPI imaging is far superior to either PI or quadratic imaging alone. This is due to the fact that applying quadratic filtering to Pulse-inversion data (in that order) allows the cascade to efficiently mitigate the limitations of either imaging method applied alone. Specifically, PI processing efficiently removes fundamental stationary tissue components, but amplifies the noise floor thus masking low-level harmonic activity and fails in suppressing echoes from moving tissue which could mask echoes from microbubbles. The quadratic kernel can be optimally designed to efficiently remove noise throughout the spectrum, maintaining quadratic data, even below the noise floor, and reducing tissue component introduced by motion.

6. REFERENCES

- [1] D. H. Simpson, C. T. Chin, and P. N. Burns, "Pulse inversion Doppler: A new method for detecting nonlinear echoes from microbubble contrast agent," *IEEE Trans. Ultrason., Ferroelect., Freq. Contr.*, vol. 46, no. 2, pp. 372-382, Mar. 1999.
- [2] P. Phukpattaranont and E. S. Ebbini, "Post-beamforming second-order Volterra filter for nonlinear pulse-echo ultrasonic imaging," *IEEE Trans. Ultrason., Ferroelect., Freq. Contr.*, vol. 50, no. 8, pp. 987-1001, Aug. 2003.
- [3] P. Phukpattaranont, M. F. Al-Mistarihi and E. S. Ebbini, "Post-beamforming Volterra filters for contrast-assisted ultrasonic imaging: In-vivo results," in *Proc. IEEE Ultrason. Symp.*, 2003.
- [4] M. F. Al-Mistarihi and E. S. Ebbini, "Quadratic Pulse Inversion Ultrasonic Imaging (QPI): Detection of Low-level Harmonic Activity of Microbubble Contrast Agents" *ICASSP05*, 2005.